Gravity Currents Produced by Sudden Release of a Fixed Volume of Heavy Fluid

S. J. D. D'Alessio, T. Bryant Moodie, J. P. Pascal, and G. E. Swaters

In this paper we study various aspects of gravity (or density) currents arising from instantaneous releases of heavy fluids in a rectangular channel with a horizontal bottom. It is shown, by means of a scaling argument, that these plane currents can be successfully modeled by a two-by-two system in conservation form together with a pair of algebraic relations. A number of numerical experiments are carried out using this "weak stratification" model to elicit information concerning the behavior of gravity currents. A weakly nonlinear analysis is employed to clarify some aspects that were uncovered by the numerical experimentation.

1. Introduction

A gravity current consists of the flow of one fluid within another when this flow is driven by the density difference between these fluids [1]. Gravity currents are primarily horizontal, occurring as either top or bottom boundary currents or as intrusions at some intermediate level, although there are important oceanic and other examples in which these currents have distinct vertical components. We here are interested in bottom boundary currents.

Address for correspondence: Professor T. Bryant Moodie, Director, Applied Mathematics Institute, Department of Mathematical Sciences, University of Alberta, Edmonton, Alberta, T6G 2G1, Canada.

STUDIES IN APPLIED MATHEMATICS 96:359–385

Published by Blackwell Publishers, 238 Main Street, Cambridge, MA 02142, USA, and 108 Cowley Road, Oxford, OX4 1JF, UK.

Gravity currents play an important role in many known natural phenomena and will likely be seen to figure prominently in other natural events as our level of understanding of them is increased.

The downdraft section of a thunderstorm produces a cold dense outflow in the form of a strong gravity current that has associated with it vertical wind shears that are of sufficient magnitude to pose a threat to commercial aircraft. The inland boundary of the sea breeze in the late afternoon has the behavior of a gravity current and has been shown in some cases to recirculate pollutants emitted near a shoreline [2]. Airborne insects, such as the spruce budworm moth in New Brunswick, Canada have been observed to be concentrated at these sea-breeze fronts [3]. Many oceanic fronts, especially those created by tidal processes, appear to be governed by simple gravity current frontal dynamics. Deep-water renewal in fjords also depends to a large extent on the gravity current mechanism [1].

Turbidity currents in the ocean whose density-difference mechanism is due to the presence of suspended particles are implicated in everything from the erosion of underwater canyons to the destruction of submarine cables and the formation of tsunamis. It has been suggested that the action of atmospheric-suspension gravity currents on the Martian landscape may be responsible for the channels observed there [4].

From what we have outlined here it is clear that gravity currents play a central role in many of the natural processes here on Earth and may also have figured prominently in shaping the physical features of several other planets. Considering the importance of gravity currents we felt that more work on them was justified.

The first theoretical calculation in the area of gravity currents was by von Kármán [5]. He gave a demonstration to show that a current of density ρ_2 and depth h propagates under a fluid of density ρ_1 $(< \rho_2)$ and of semi-infinite depth at a speed c where

$$c = (2g'h)^{1/2} \tag{1.1}$$

with the reduced gravity $g' = g(\rho_2 - \rho_1)/\rho_1$, where g is the acceleration due to gravity. Benjamin [6] subsequently explained that von Kármán's reasoning in arriving at (1.1) was incorrect but that the result, for this restricted problem, was nevertheless true. Benjamin [6] studied steady irrotational gravity currents in perfect fluids having a fixed upper boundary by regarding the overall balance to be between horizontal momentum and the hydrostatic force. Using this simple model he was able to achieve some broad agreement with the earlier experiments of Keulegan [7].

One of the first numerical studies of density currents was by Daly and Pracht [8] who employed the marker and cell technique to examine flows with density ratios varying from 1.05 to 3.0. They obtained reasonable agreement with Middleton's [9] experimentally determined front position versus

time data for flows in which the density interface initially extends to the upper surface of the flow regime. Kao et al. [10] employed a finite difference scheme to solve numerically the equations for viscous, diffusive, two-dimensional laminar flows modeling both the overflow and the underflow cases in an ambient fluid of finite depth having a "rigid lid." Their work points clearly to the fact that for regions of finite total depth the motions of the fluid surrounding the current are important to the overall analysis. Huppert and Simpson [11] presented an analysis for the gravity current arising from the release of a fixed volume of one homogeneous fluid into another of slightly different density. Their analysis assumes that a gravity current slumps through a series of two-dimensional rectangles of equal volume and that the collapse is controlled at the head. Using these simple ideas they were able to predict the position of the front of the current as a function of time achieving reasonable agreement with their and Keulegan's [12] experiments.

Rottman and Simpson [13] considered the instantaneous release of a finite volume of homogeneous fluid into another fluid of slightly lower density. Modeling their system by means of a two-layer fluid bounded above and below by rigid horizontal planes and employing the Boussinesq approximation they came up with a two-by-two system which could be put into characteristic form. They performed experiments designed to throw light on the initial adjustment phase of the flow and its transition to the self-similar phase. They argued that this transition occurs when a disturbance generated at the end-wall overtakes the front. They observed that the form of this disturbance was a function of the fractional depth occupied by the heavy fluid. Grundy and Rottman [14] studied the known similarity solutions to a version of the shallow-water equations and demonstrated by means of numerical computations that they constitute the large-time limits of the solutions of initial value problems for these equations.

In this article we examine various aspects of gravity currents basing our analysis on a two-layer fluid model. The full shallow-water equations are derived in Section 2. Then in Section 3 we establish a simplified asymptotic form of these equations. In Section 4 we compare results for initial value problems obtained from the full and aysmptotic equations and go on to employ these model equations in various numerical experiments. In Section 5 we use multiple scale arguments to more fully understand the mechanisms that are captured by these model equations. A concluding discussion is presented in Section 6.

2. Formulation

The physical configuration of our two-layer fluid model is depicted in Figure 1. In Figure 1, $\eta(x, y, t)$ represents the displacement of the free surface

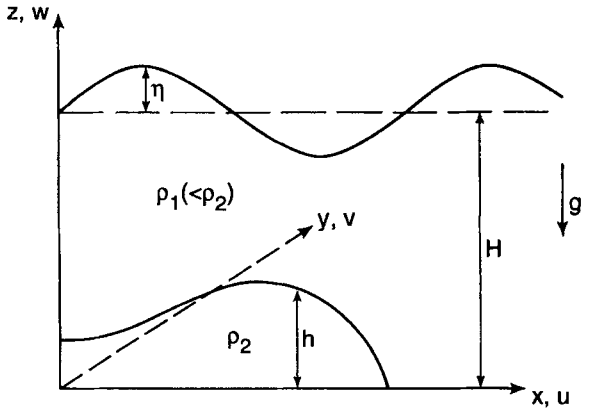

Figure 1. A sketch of the two-layer fluid model for gravity currents.

from its undisturbed configuration, $\boldsymbol{u} = (u, v, w)$ is the fluid velocity in Cartesian coordinates with position vector $\boldsymbol{x} = (x, y, z)$, H is the mean total depth, $h(x, y, t)$ is the thickness of the underlying fluid, and ρ_1, ρ_2 $(\rho_1 < \rho_2)$ represent the constant densities of the upper and lower fluids, respectively.

The equations of motion for a fluid in a nonrotating frame consist of the continuity equation

$$\frac{D\rho}{Dt} + \rho \nabla \cdot \boldsymbol{u} = 0, \tag{2.1}$$

and the equation of momentum balance, that is,

$$\rho \frac{D\boldsymbol{u}}{Dt} = -\nabla p + \rho \nabla \varphi + \boldsymbol{F}(\boldsymbol{u}), \tag{2.2}$$

wherein

$$\frac{D}{Dt} \equiv \frac{\partial}{\partial t} + \boldsymbol{u} \cdot \nabla \tag{2.3}$$

is the material derivative, p is the total fluid pressure, φ is the potential by which conservative body forces such as gravity can be represented, and $\boldsymbol{F}$ is any nonconservative force. We take the two fluids to be inviscid and incompressible so that the equation of mass conservation (2.1) reduces to the incompressibility condition

$$\nabla \cdot \boldsymbol{u} = 0 \tag{2.4}$$

in each layer and $\boldsymbol{F} \equiv \boldsymbol{0}$ in (2.2). We take the sole conservative body force to be that of gravity and neglect the effects of surface tension at the interface and at the front, or contact line. This latter condition requires that the Bond number $B = \rho_2 g' L^2/\sigma \gg 1$, where $g' = (\rho_2 - \rho_1)g/\rho_2$ is the reduced gravity,

L the length of the current, and σ the surface tension. We now adapt these equations to the study of a system consisting of two coupled layers overlying a flat bottom.

The momentum equations for the upper layer when written in component form are

$$\frac{\partial u_1}{\partial t} + u_1 \frac{\partial u_1}{\partial x} + v_1 \frac{\partial u_1}{\partial y} + w_1 \frac{\partial u_1}{\partial z} = -\frac{1}{\rho_1} \frac{\partial \tilde{p}_1}{\partial x}, \tag{2.5a}$$

$$\frac{\partial v_1}{\partial t} + u_1 \frac{\partial v_1}{\partial x} + v_1 \frac{\partial v_1}{\partial y} + w_1 \frac{\partial v_1}{\partial z} = -\frac{1}{\rho_1} \frac{\partial \tilde{p}_1}{\partial y}, \tag{2.5b}$$

$$\frac{\partial w_1}{\partial t} + u_1 \frac{\partial w_1}{\partial x} + v_1 \frac{\partial w_1}{\partial y} + w_1 \frac{\partial w_1}{\partial z} = -\frac{1}{\rho_1} \frac{\partial \tilde{p}_1}{\partial z}, \tag{2.5c}$$

where the total pressure p_1 in the upper layer has been written as

$$p_1(x, y, z, t) = -\rho_1 g z + \tilde{p}_1(x, y, z, t), \tag{2.6}$$

the first part of which cancels the constant gravitational force per unit mass in the fluid. Standard scaling arguments [15] show that to $O(\delta^2)$, where δ is the aspect ratio, that is,

$$\delta \equiv H/L \ll 1, \tag{2.7}$$

$\partial \tilde{p}_1/\partial z$ is negligible, that is,

$$\frac{\partial p_1}{\partial z} = -\rho_1 g + O(\delta^2). \tag{2.8}$$

This is the hydrostatic approximation that applies to thin layers of fluid.

Integrating (2.8) and applying the boundary condition at the free surface gives

$$p_1 = \rho_1 g[(H + \eta) - z] + p_0, \tag{2.9}$$

where p_0 is a constant that may be equated to zero. From (2.9) we have that the horizontal pressure gradients and hence the horizontal velocities are independent of z so that the horizontal momentum equations then become

$$\frac{\partial u_1}{\partial t} + u_1 \frac{\partial u_1}{\partial x} + v_1 \frac{\partial u_1}{\partial y} = -g \frac{\partial \eta}{\partial x}, \tag{2.10a}$$

$$\frac{\partial v_1}{\partial t} + u_1 \frac{\partial v_1}{\partial x} + v_1 \frac{\partial v_1}{\partial y} = -g \frac{\partial \eta}{\partial y}. \tag{2.10b}$$

The condition that u_1, v_1 are independent of z allows the continuity equation (2.4) to be integrated in z in the upper layer yielding

$$w_1(x, y, z, t) = -z\left(\frac{\partial u_1}{\partial x} + \frac{\partial v_1}{\partial y}\right) + \tilde{\omega}_1(x, y, t). \tag{2.11}$$

Applying the kinematic condition at the boundary between the lighter and heavier fluids, that is,

$$\frac{D}{Dt}(z-h)=0, \tag{2.12}$$

and using this result in (2.11) gives

$$\tilde{\omega}_1=\frac{\partial h}{\partial t}+h\left(\frac{\partial u_1}{\partial x}+\frac{\partial v_1}{\partial y}\right)+\frac{\partial h}{\partial x}u_1+\frac{\partial h}{\partial y}v_1 \tag{2.13}$$

so that

$$w_1=(h-z)\left(\frac{\partial u_1}{\partial x}+\frac{\partial v_1}{\partial y}\right)+\frac{\partial h}{\partial x}u_1+\frac{\partial h}{\partial y}v_1+\frac{\partial h}{\partial t}. \tag{2.14}$$

Combining (2.14) with the kinematic condition of the upper surface yields the continuity equation for the upper layer as

$$\frac{\partial}{\partial t}(\eta-h)+\nabla_H\cdot[(H+\eta-h)\boldsymbol{u}_1]=0, \tag{2.15}$$

where we have introduced the horizontal divergence operator $\nabla_H\equiv(\partial_x,\partial_y)$.

Performing similar calculations for the lower layer and using the condition of zero normal velocity at the horizontal bottom and the kinematic condition at the interface we readily obtain the momentum equation,

$$\frac{\partial \boldsymbol{u}_2}{\partial t}+(\boldsymbol{u}_2\cdot\nabla_H)\boldsymbol{u}_2+\frac{1}{\rho_2}\nabla_H\tilde{p}_2=\boldsymbol{0}, \tag{2.16}$$

and the continuity equation,

$$\frac{\partial h}{\partial t}+\nabla_H\cdot(h\boldsymbol{u}_2)=0, \tag{2.17}$$

where, as in the upper layer, we have decomposed the total pressure p_2 in the form

$$p_2=-\rho_2 gz+\tilde{p}_2(x,y,z,t). \tag{2.18}$$

The momentum and conservation equations for the two-layer model consisting of (2.10), (2.15), (2.16), and (2.17) comprise a set of six equations in the seven unknowns $\boldsymbol{u}_1$, η, h, $\boldsymbol{u}_2$, and $\tilde{p}_2$. To close this system we need an additional condition. We obtain this by requiring that total pressure be continuous across the interface. The pressure field in the lower layer, which matches across the interface with that in the upper layer, is

$$p_2=-\rho_2 gz+\rho_1 gH+\rho_1 g\eta+\rho_2 g'h. \tag{2.19}$$

Hence we have that

$$\tilde{p}_2(x, y, t) = \rho_1 g H + \rho_1 g \eta + \rho_2 g' h. \tag{2.20}$$

In summary our system of equations for the two-layer fluid system having a horizontal lower boundary consists of

$$\frac{\partial \boldsymbol{u}_1}{\partial t} + (\boldsymbol{u}_1 \cdot \nabla_H)\boldsymbol{u}_1 + g\nabla_H \eta = \mathbf{0}, \tag{2.21a}$$

$$\frac{\partial}{\partial t}(\eta - h) + \nabla_H \cdot [(H + \eta - h)\boldsymbol{u}_1] = 0, \tag{2.21b}$$

$$\frac{\partial \boldsymbol{u}_2}{\partial t} + (\boldsymbol{u}_2 \cdot \nabla_H)\boldsymbol{u}_2 + (g - g')\nabla_H \eta + g'\nabla_H h = \mathbf{0}, \tag{2.21c}$$

$$\frac{\partial h}{\partial t} + \nabla_H \cdot (h\boldsymbol{u}_2) = 0. \tag{2.21d}$$

3. Preliminary analysis

We now carry out some preliminary analysis with the aim of developing and, in the next section, testing an asymptotic version of the system (2.21) for use in analyzing typical gravity flow situations. In all instances we are interested in plane flow situations so that the set of six equations in (2.21) reduces to the four-by-four system

$$\frac{\partial u_1}{\partial t} + u_1 \frac{\partial u_1}{\partial x} + g \frac{\partial \eta}{\partial x} = 0, \tag{3.1a}$$

$$\frac{\partial}{\partial t}(\eta - h) + \frac{\partial}{\partial x}[(H + \eta - h)u_1] = 0, \tag{3.1b}$$

$$\frac{\partial u_2}{\partial t} + u_2 \frac{\partial u_2}{\partial x} + g \frac{\partial \eta}{\partial x} + g' \frac{\partial}{\partial x}(h - \eta) = 0, \tag{3.1c}$$

$$\frac{\partial h}{\partial t} + \frac{\partial}{\partial x}(hu_2) = 0. \tag{3.1d}$$

We now nondimensionalize the system (3.1) using a scaling that focuses on the nonlinear internal gravity wave processes. To this end we introduce the nondimensional quantities signified by a tilde according to

$$\begin{aligned} \eta &= \tfrac{g'}{g} H\tilde{\eta}, \qquad & (u_1, u_2) &= (\tilde{u}_1, \tilde{u}_2)(g'H)^{1/2}, \\ h &= H\tilde{h}, & L/T &= (g'H)^{1/2}, \end{aligned} \tag{3.2}$$

where L is a horizontal length scale and T a time scale which are then to be chosen so that their ratio gives $(g'H)^{1/2}$. Under this advective scaling the

nondimensional equations are

$$(\partial_t + u_1\partial_x)u_1 + \eta_x = 0, \tag{3.3a}$$

$$(g'\eta/g - h)_t + [(1 + g'\eta/g - h)u_1]_x = 0, \tag{3.3b}$$

$$(\partial_t + u_2\partial_x)u_2 + \eta_x + (h - g'\eta/g)_x = 0, \tag{3.3c}$$

$$h_t + (hu_2)_x = 0, \tag{3.3d}$$

where tildes have been dropped for notational convenience.

If we now neglect all terms of $O(g'/g)$ on the assumption that density differences are small, our system of model equations then becomes

$$(\partial_t + u_1\partial_x)u_1 + \eta_x = 0, \tag{3.4a}$$

$$-h_t + [(1 - h)u_1]_x = 0, \tag{3.4b}$$

$$(\partial_t + u_2\partial_x)u_2 + \eta_x + h_x = 0, \tag{3.4c}$$

$$h_t + (hu_2)_x = 0. \tag{3.4d}$$

This system can be reduced to a two-by-two system together with two algebraic relations. Adding (3.4b) and (3.4d) and integrating gives

$$(1 - h)u_1 + hu_2 = 0. \tag{3.5}$$

This condition specifies no net mass flux. Then, multiplying (3.4a) by $(1 - h)$ and adding this to u_1 times (3.4b) gives

$$[(1 - h)u_1]_t + [(1 - h)u_1^2]_x + (1 - h)\eta_x = 0. \tag{3.6}$$

Multiply (3.4c) by h and add this to u_2 times (3.4d) to get

$$(hu_2)_t + (hu_2^2)_x + h\eta_x + hh_x = 0. \tag{3.7}$$

Add (3.6) and (3.7) and employ (3.5) to get the condition for no net flux of linear momentum, that is,

$$(1 - h)u_1^2 + hu_2^2 + \eta + \tfrac{1}{2}h^2 = 0. \tag{3.8}$$

This equation then provides an expression for η, that is,

$$\eta = -\frac{1}{2}h^2 - \frac{hu_2^2}{1 - h} < 0. \tag{3.9}$$

Our model system for $g'/g \ll 1$ is thus given by the two-by-two system $(u_2 \equiv u)$

$$u_t + (u + \eta_u)u_x + (1 + \eta_h)h_x = 0, \tag{3.10a}$$

$$h_t + (hu)_x = 0, \tag{3.10b}$$

together with the algebraic relations

$$\eta = \eta(u, h) = -\frac{1}{2}h^2 - \frac{hu^2}{1-h}, \tag{3.11}$$

$$u_1 = \frac{hu}{h-1}. \tag{3.12}$$

Defining the vector of state variables by

$$\boldsymbol{U} \equiv \begin{bmatrix} u \\ h \end{bmatrix} \tag{3.13}$$

enables us to cast our two-by-two system into conservation form as

$$\boldsymbol{U}_t + [\boldsymbol{f}(\boldsymbol{U})]_x = \boldsymbol{0}, \tag{3.14}$$

where the vector-valued flux function $\boldsymbol{f}$ is given by

$$\boldsymbol{f} \equiv \begin{bmatrix} \frac{1}{2}u^2 + h + \eta(u, h) \\ hu \end{bmatrix}. \tag{3.15}$$

The eigenvalues associated with (3.14) are $\lambda^{\pm}$, where

$$\lambda^{\pm} = \frac{u(1-2h)}{1-h} \pm \frac{1}{1-h}\sqrt{h(1-h)[(1-h)^2 - u^2]}. \tag{3.16}$$

The system is hyperbolic where $\lambda^{\pm}$ are real. The region of hyperbolicity is depicted in Figure 2.

Associated with the system (3.14) are the left and right eigenvectors $\boldsymbol{\ell}^{\pm}$ and $\boldsymbol{r}^{\pm}$ satisfying the orthonormality conditions

$$\boldsymbol{\ell}^{\pm} \cdot \boldsymbol{r}^{\mp} = 0, \qquad \boldsymbol{\ell}^{\pm} \cdot \boldsymbol{r}^{\pm} = 1, \tag{3.17}$$

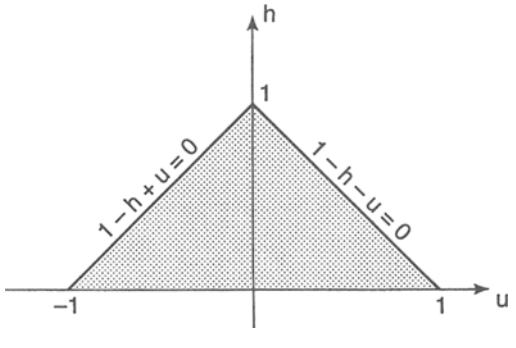

Figure 2. Region of hyperbolicity in the (u, h)-plane.

namely

$$\ell^{\pm} = \left[1,\ \frac{1}{h}(\lambda^{\pm} - u) + \frac{2u}{1-h}\right] \tag{3.18}$$

and

$$r^{\pm} = \frac{(1-h)h}{2[(1-h)(\lambda^{\pm} - u) + uh]}\begin{bmatrix}(\lambda^{\pm} - u)/h \\ 1\end{bmatrix}. \tag{3.19}$$

To determine the nonlinear nature of the characteristic fields $\lambda^{\pm}(U)$ we must calculate their gradients in the $r^{\pm}$ directions, that is,

$$\operatorname{grad}_U \lambda^{\pm} \cdot r^{\pm}. \tag{3.20}$$

The characteristic field is called *genuinely nonlinear* [16] if the expression in (3.20) is nonvanishing and *linearly degenerate* if this expression is zero. The nonvanishing of this expression implies the formation of a caustic envelope for the associated family of characteristics and the generation of shocks [17]. Some straightforward calculations give

$$\begin{aligned}\operatorname{grad}_U \lambda^{\pm} \cdot r^{\pm} = {} & \left[\frac{\mp uh}{2\sqrt{h(1-h)[(1-h)^2 - u^2]}} + \frac{1}{2}\right] \\ & \left[\frac{1-2h}{1-h} \mp \frac{uh}{\sqrt{h(1-h)[(1-h)^2 - u^2]}}\right] \\ & + \frac{h}{2\sqrt{h(1-h)[(1-h)^2 - u^2]}} \\ & \left[\frac{\mp u}{1-h} + \frac{\sqrt{h(1-h)[(1-h)^2 - u^2]}}{1-h}\right. \\ & \left. + \frac{(1-h)^3 - 3h(1-h)^2 - u^2(1-2h)}{2\sqrt{h(1-h)[(1-h)^2 - u^2]}}\right].\end{aligned} \tag{3.21}$$

We discuss some of the implications that may be drawn from (3.21) in the section on numerical results and also in Section 5, which is devoted to a perturbation analysis. However, it should be pointed out here that our characteristic fields are locally linearly degenerate [18] about the state $u = 0$, $h = \frac{1}{2}$, that is,

$$\operatorname{grad}_U \lambda^{\pm} \cdot r^{\pm}\Big|_{\substack{u=0 \\ h=1/2}} = 0. \tag{3.22}$$

This degeneracy will resurface in future shock calculations.

In the next section we compare numerical results for a selection of initial value problems to demonstrate that our two-by-two system of model equations captures all of the essential dynamics of gravity flows as modeled by the full four-by-four system. After establishing this validity various numerical experiments are carried out and discussed.

4. Numerical results

Numerical solutions to the full four-by-four system of conservation laws (3.1a)–(3.1d) and the model equations (3.10)–(3.12) were obtained using MacCormack's method [19]. This method is an explicit conservative finite-difference scheme possessing second-order accuracy. Because the scheme is conservative, convergence will be to a physical weak solution of the hyperbolic system of equations. Further, MacCormick's method provides sharp resolution of shocks and does not require the evaluation of the Jacobian of the flux vector. One drawback is the occurrence of oscillations around the shock. However, these can be adequately damped by applying artificial viscosity. This is done by introducing a numerical diffusion term proposed by Lapidus [20].

MacCormick's method for solving the hyperbolic system

$$\boldsymbol{U}_t + \boldsymbol{F}(\boldsymbol{U})_x = \boldsymbol{0}, \tag{4.1}$$

is a two-step procedure that first uses forward differencing followed by backward differencing to achieve second-order accuracy. The scheme is given by

$$U_j^* = U_j^n - \frac{k}{h}\left(F(U_{j+1}^n) - F(U_j^n)\right), \tag{4.2a}$$

$$U_j^{n+1} = \frac{1}{2}\left(U_j^n + U_j^*\right) - \frac{k}{2h}\left(F(U_j^*) - F(U_{j-1}^*)\right). \tag{4.2b}$$

In the above, k denotes the increment in time while h refers to the equal spacing of grid points in the x direction. Here, we have adopted the notation $U_j^n = U(x_j, t_n)$.

The particular physical problem that was considered in connection with the two systems of equations (3.1)–(3.1d) and (3.10)–(3.12) is that of the instantaneous release of a rectangular-shaped fixed volume of denser fluid initially at rest into a channel containing the less dense fluid. It is assumed that a solid boundary is located at the left end of the channel ($x = 0$) and that the channel is semi-infinite so that the fluid at large distances is taken to remain undisturbed. The resulting initial conditions can then be written as

$$u_1(x, 0) = 0, \qquad u_2(x, 0) = 0, \qquad \eta(x, 0) = 0,$$

$$h(x, 0) = \begin{cases} h_0 & \text{for } x \le x_0, \\ 0 & \text{for } x > x_0, \end{cases} \tag{4.3}$$

where $x_0 = 1$ was used in all the computations. The boundary conditions are given by

$$\begin{aligned} u_1(0, t) &= 0, \qquad u_2(0, t) = 0, \qquad t > 0, \\ h_x(0, t) &= 0, \qquad \eta_x(0, t) = 0, \qquad t > 0. \end{aligned} \tag{4.4}$$

The flux conditions for h and η can be expected from symmetry arguments and can be derived from the governing equations using the impermeability conditions.

The validity of the simplified model equations can best be demonstrated by comparing the results with those obtained from the full four-by-four system. Such comparisons are illustrated in Figures 3a and 3b for the gravity current for various values of the dimensionless parameter (g'/g). As expected, these diagrams reveal that the agreement improves as g'/g is decreased. The case of large h_0, which is illustrated in Figure 3a, constitutes the worst scenario with regard to the agreement between the two systems. As indicated in Figure 3b, the agreement improves as h_0 is decreased.

With regard to the results for the free surface, the comparison of the solutions of the two systems is presented in Figure 4. It can be seen that the solution to the four-by-four system indicates that the disturbance of the free surface is composed of a depression and a surface gravity wave propagating to the right. The observation that at a given time the amount by which the free surface is depressed equals the amount by which it is elevated can be analytically substantiated by the fact that

$$\int_0^\infty \eta(x, t)dx = 0, \qquad t > 0.$$

The above result can be easily obtained from Equations (3.1b) and (3.1d).

The results illustrated in Figure 4 suggest better agreement between the two systems for the depressed region of the free surface as g'/g decreases. Examining the expression for η, we discover that the model equations will always yield a depression as η is strictly negative. Further, the solution to the model equations does not show the existence of the surface gravity wave. This is to be expected since the model equations were derived on the assumption that g'/g vanishes, in which case the surface gravity waves propagate with infinite velocity and are therefore filtered out of the solutions of the model equations. It turns out that g'/g is related to the ratio of the speed of surface gravity waves to that of internal gravity waves; thus as $(g'/g) \to 0$ the surface gravity waves propagate infinitely faster than the internal gravity waves.

It is judged from the above-mentioned comparisons that the model equations predict the essential features of the gravity current and free surface and therefore justify using it in place of the full four-by-four system. Thus, whenever we speak of numerical solutions in what follows, it is implied that these were obtained from the model equations.

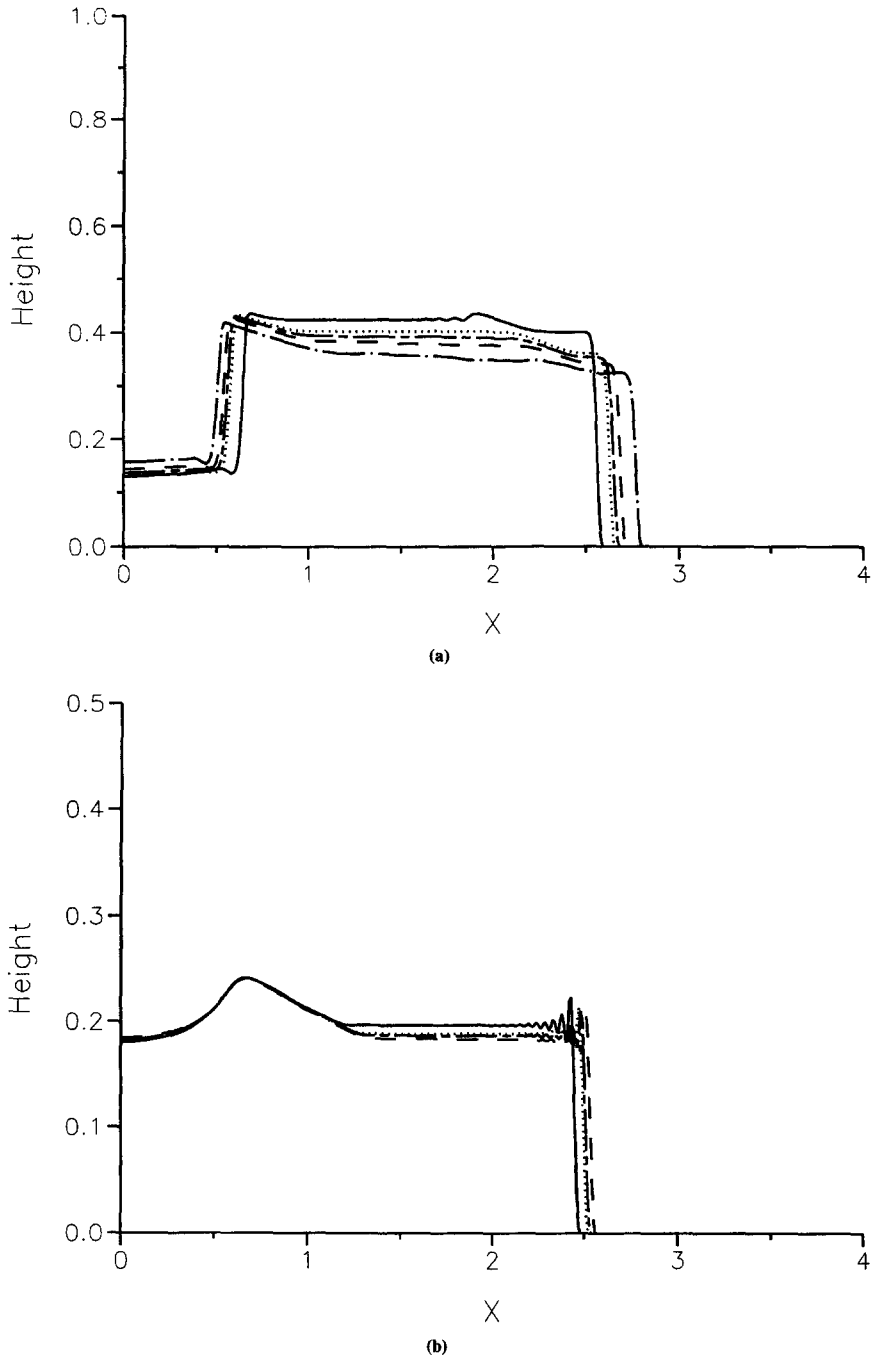

Figure 3. Comparison of the gravity current predicted by the model equations with that of the full equations for **(a)** various g'/g ratios with $h_0 = .9$ at $t = 3$ and **(b)** various g'/g ratios with $h_0 = .5$ at $t = 3$.

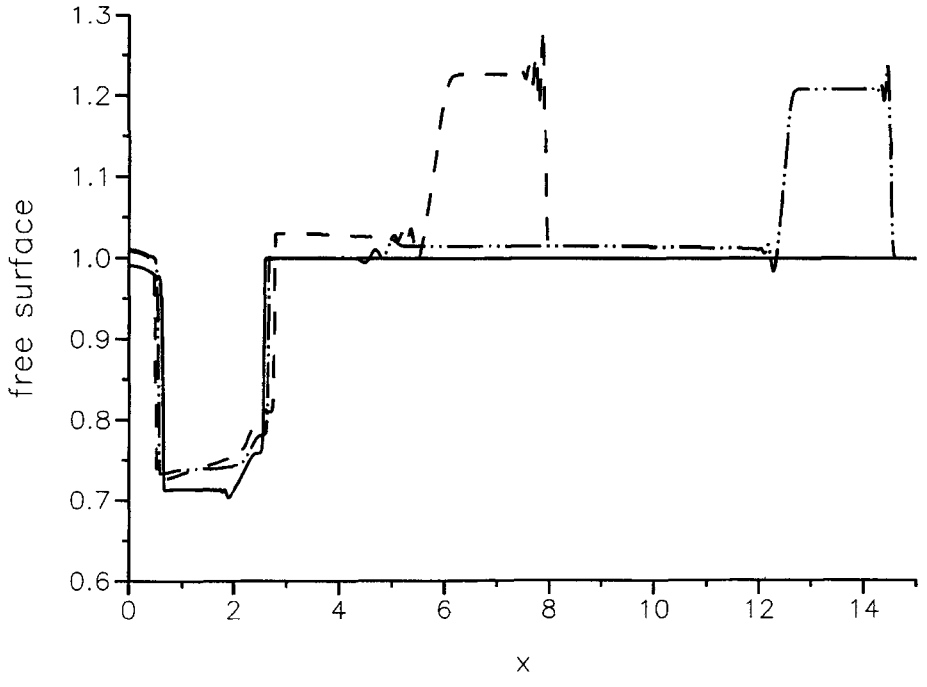

Figure 4. Comparison of the free surface predicted by the model equations with that of the full equations for various g'/g ratios with $h_0 = 0.9$ at $t = 3$.

Several checks were made on the numerical results. One of these consisted of computing the volume of the denser fluid (i.e., the gravity current) at each time step. In accordance with conservation of mass, the volume was found to remain constant.

The numerical results were also compared to similarity solutions. In the event that the denser fluid layer is much thinner than the less dense fluid (i.e., $h_0 \ll 1$) the effect on the free surface is negligible (i.e., $\eta \approx 0$). As a consequence of this, the four-by-four system collapses to

$$\frac{\partial u_2}{\partial t} + \frac{\partial}{\partial x}\left(\frac{1}{2}u_2^2 + h\right) = 0, \tag{4.5a}$$

$$\frac{\partial h}{\partial t} + \frac{\partial}{\partial x}(hu_2) = 0. \tag{4.5b}$$

It can be shown [21, 22] that the above equations possess similarity solutions of the form

$$u_2(x, t) = t^{-1/3}v(\xi), \tag{4.6a}$$

$$h(x, t) = t^{-2/3}f(\xi), \tag{4.6b}$$

where

$$v(\xi) = \tfrac{2}{3}\,\xi, \tag{4.7a}$$

$$f(\xi) = \tfrac{1}{9}\,(\xi^2 + \xi_1^2), \tag{4.7b}$$

$$\xi = xt^{-2/3}, \tag{4.7c}$$

and

$$\xi_1 = 3\left(\frac{h_0 x_0}{4}\right)^{1/3}. \tag{4.7d}$$

The shock front location x_f is given by

$$x_f(t) = 3\left(\frac{h_0 x_0}{4}\right)^{1/3} t^{2/3} \tag{4.8}$$

beyond which u_2 and h are zero. These solutions can be interpreted as the leading terms of an asymptotic expansion for large t.

Figure 5 compares the similarity solutions with the numerical solutions at different times for $h_0 = 0.5$. It is clear that the agreement is better for larger

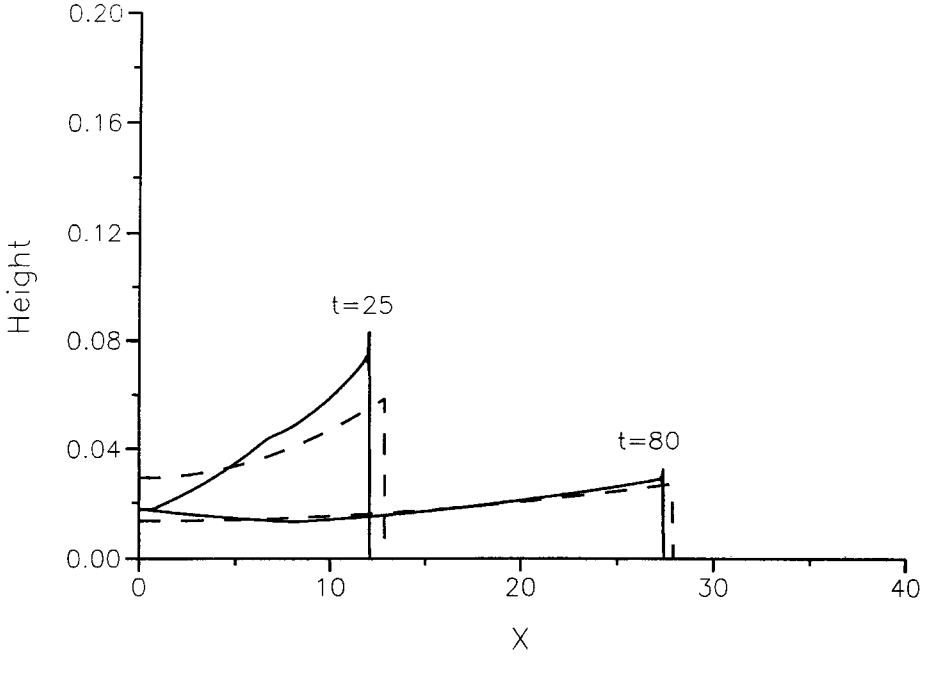

Figure 5. Comparison of the gravity current obtained by the model equations with the similarity solutions for times $t = 25$ and $t = 80$ with $h_0 = 0.5$.

times as to be expected. A similar conclusion can be drawn from Figure 10, which displays the location of the front for various values of h_0. It can be further observed that as h_0 decreases the agreement improves. This is due to the fact that the similarity solutions best model the physics for $h_0 \ll 1$.

As another check on our numerical results, the model equations were also solved by a method developed recently by Glaister [23]. This method can be classified as a Godunov-type method and is successful in dealing with systems containing source terms. The model equations can be written in vector form as

$$\begin{pmatrix} u \\ h \end{pmatrix}_t + \begin{pmatrix} u^2/2 + h \\ uh \end{pmatrix}_x = \begin{pmatrix} -\eta_x \\ 0 \end{pmatrix}, \tag{4.9}$$

where

$$\eta_x = -\frac{2hu}{(1-h)}\, u_x - \left(h + \frac{u^2}{(1-h)^2}\right) h_x. \tag{4.10}$$

If we treat the quantity $-\eta_x$ as a source term, then Glaister's method can be applied. Displayed in Figure 6 is a comparison between the results obtained by MacCormack's method and Glaister's method. Agreement among the two

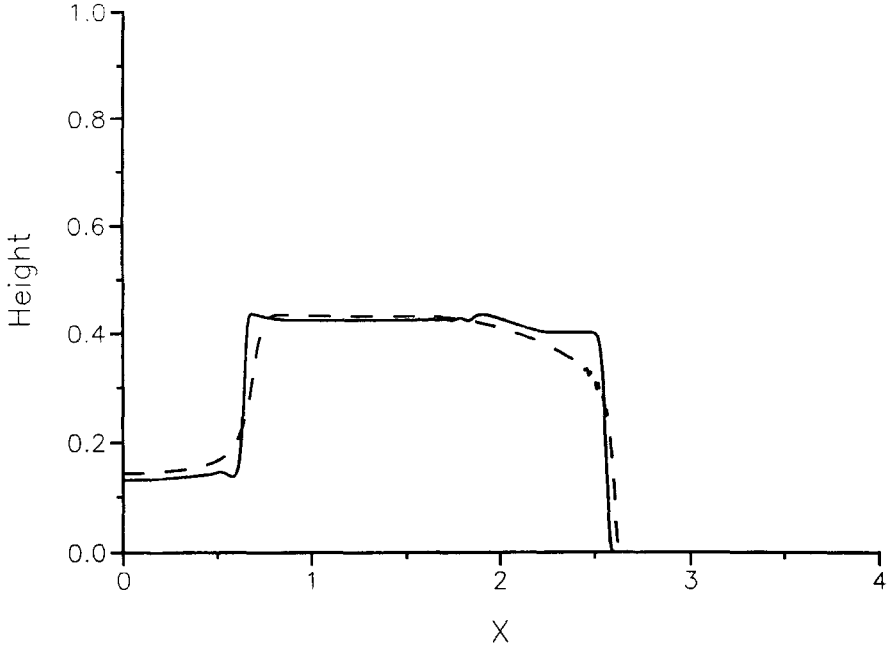

Figure 6. Comparison of the numerical results using two methods with $h_0 = 0.9$ at $t = 3$.

methods is quite good. Deviations occur near the shocks. This is because Glaister's method is first order and thus tends to smear the shocks.

As a concluding remark concerning the numerical techniques, we add that the model equations can also be solved by the method of characteristics. To use this method we rewrite the model equations in characteristic form

$$\frac{du}{dt} + \left\{ \frac{u}{1-h} \pm \sqrt{\frac{1-h}{h}} \sqrt{1 - \frac{u^2}{(1-h)^2}} \right\} \frac{dh}{dt} = 0, \tag{4.11}$$

$$\text{along} \quad \frac{dx}{dt} = \frac{u(1-2h)}{1-h} \pm \sqrt{h(1-h)} \sqrt{1 - \frac{u^2}{(1-h)^2}}. \tag{4.12}$$

Further, it can be shown that the above can also be written in the form

$$\begin{aligned} &\frac{d}{dt} \left\{ \arcsin\left(\frac{u}{1-h}\right) \pm \arcsin\left(2\left(h - \frac{1}{2}\right)\right) \right\} = 0 \\ &\text{along} \quad \frac{dx}{dt} = \frac{u(1-2h)}{1-h} \pm \sqrt{h(1-h)} \sqrt{1 - \frac{u^2}{(1-h)^2}}. \end{aligned} \tag{4.13}$$

Expressed this way it is clear that the Riemann invariants associated with the equations in characteristic form are

$$R_{\pm} = \left\{ \arcsin\left(\frac{u}{1-h}\right) \pm \arcsin\left(2\left(h - \frac{1}{2}\right)\right) \right\}. \tag{4.14}$$

Let us now interpret our numerical results and thus draw certain conclusions regarding the physical mechanisms that are operative in gravity currents. In Figure 7 we show how the structure of the gravity current depends on the initial height h_0 of the heavy fluid. It appears from the sequence of plots for the density interface with h_0 varying from 0.3 to 0.6 that a rear shock will form when $h_0 \gtrsim 0.5$. This nonlinear behavior leading to the formation of the rear shock appears to not be operational for $h_0 \lesssim 0.5$. This may be due to the lower reverse flow velocities in the upper layer as h_0 is decreased below 0.5. This value $h_0 = 0.5$ will resurface in the next section and has already appeared in (3.22) showing that both characteristic fields are linearly degenerate about $u = 0$, $h = 0.5$.

In Figure 8 the evolution in time of the gravity current is illustrated with $h_0 = 0.9$. We note that with this value of h_0 a shock is also formed at the trailing edge of the head. The calculations also reveal that the trailing shock

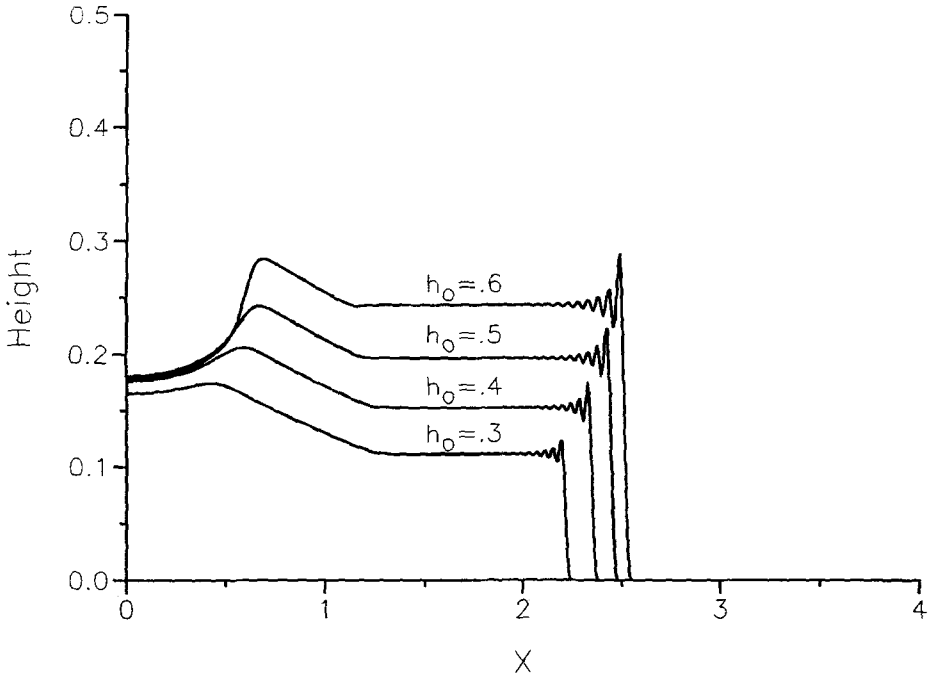

Figure 7. Dependence of the structure of the gravity current with h_0 at $t = 3$.

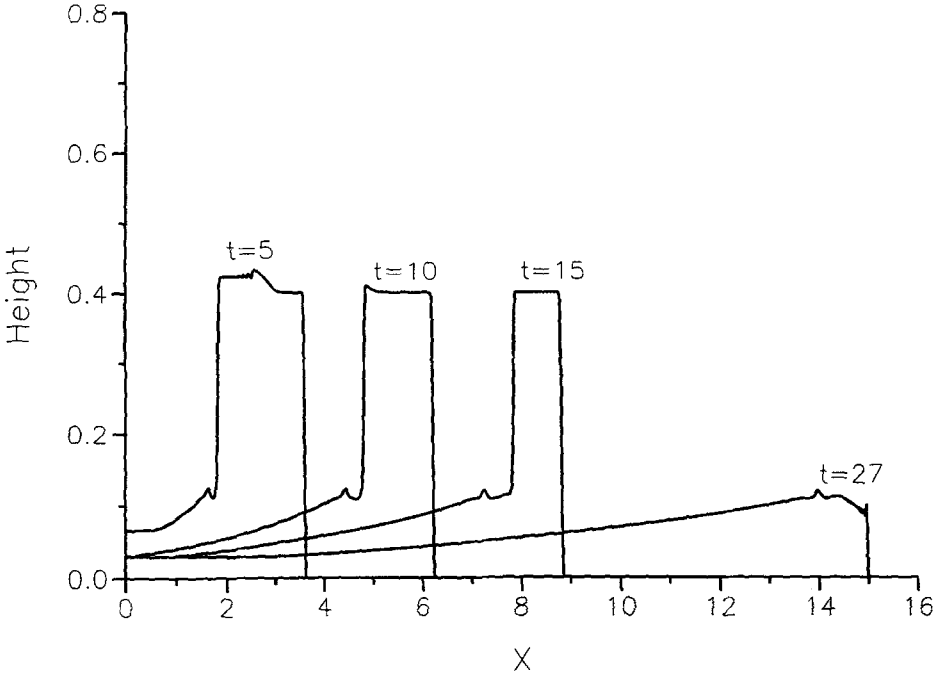

Figure 8. Time evolution of the gravity current with $h_0 = 0.9$.

travels faster than the leading front causing the head to become reduced in its horizontal dimension. At a nondimensional time $t \approx 27$, the trailing shock catches up to the front and from then on the height of the head, which until this time has remained fairly constant, begins to decrease. Furthermore, the velocity of the front, which up to this point has been fairly constant, also begins to decrease. Figure 9 tracks the positions of the trailing shock and the front in time. The decrease in the velocity of the front is indicated by a decay in the curve slope of the front position as a function of time. It can be seen that the onset of this decay coincides with the overtaking of the front by the trailing shock.

The effect of h_0 on the motion of the leading front can be determined from Figure 10. The results presented in this diagram reveal that the velocity of the front is an increasing function of h_0, and moreover, the onset of the decay of the velocity in time is delayed as h_0 increases.

Figure 11 portrays the effect of h_0 on the free surface. It is expected that the smaller the initial height of the denser fluid (i.e., the smaller h_0), the less the disturbance on the free surface. This expectation is confirmed by our results since Figure 11 indicates that the depression on the free surface decreases as h_0 is decreased.

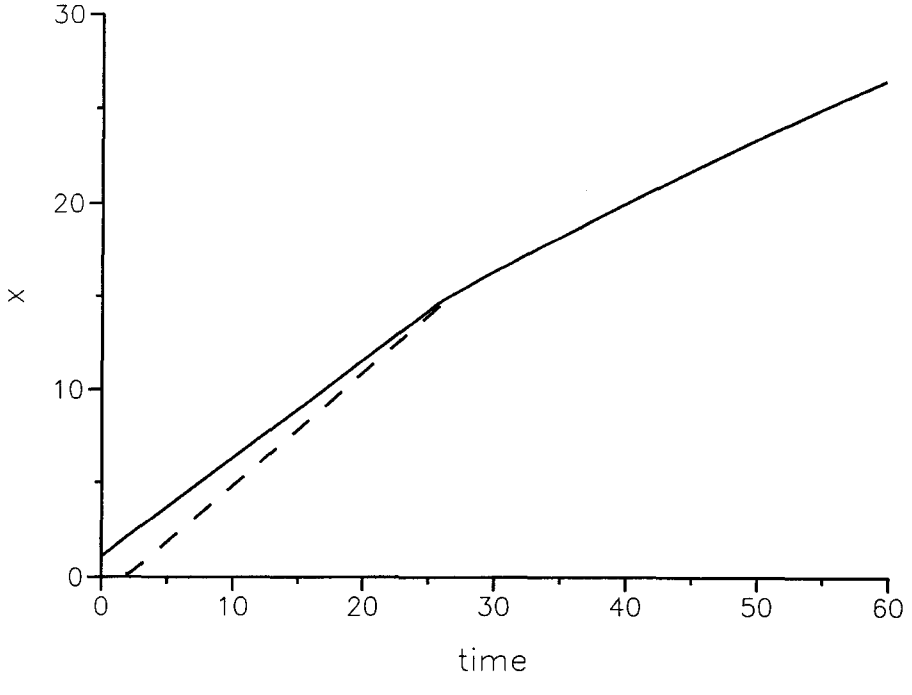

Figure 9. Location of rear shock relative to front as a function of time with $h_0 = 0.9$.

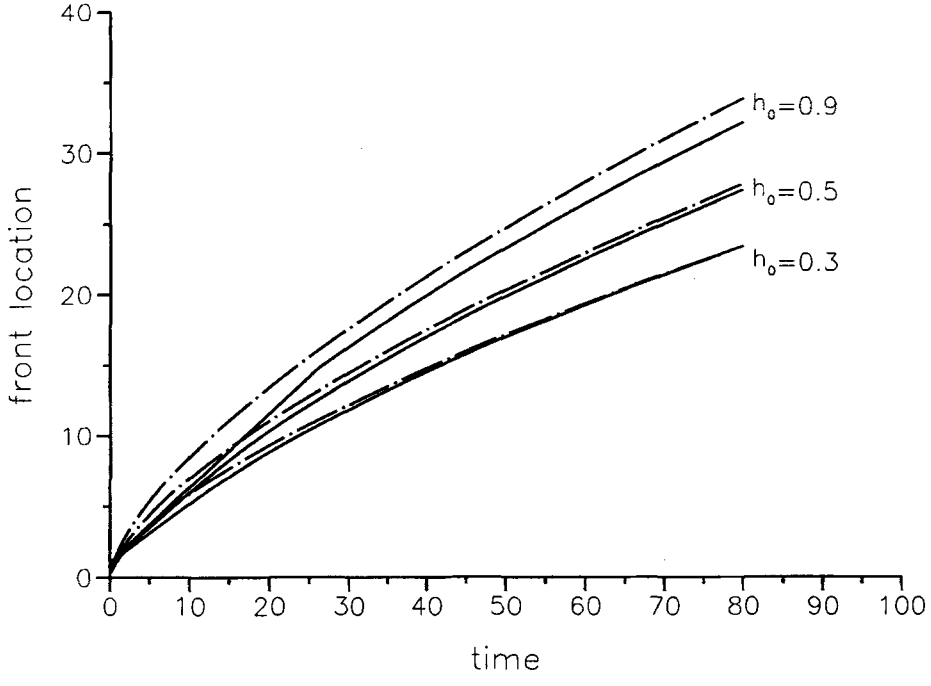

Figure 10. Front location with time for various h_0 and comparison with similarity solutions.

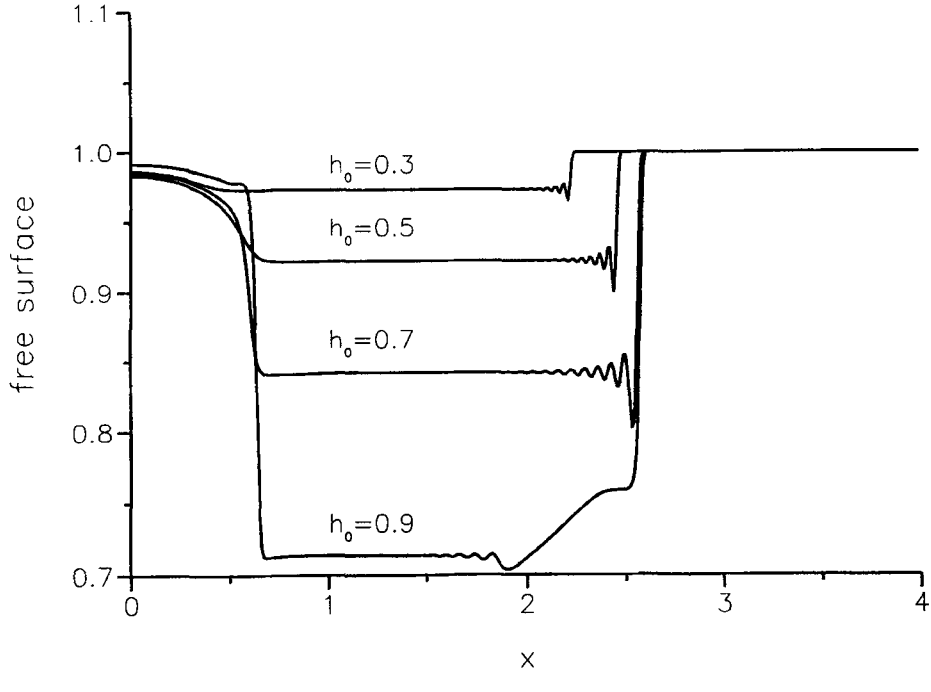

Figure 11. Dependence of free surface with h_0 at $t = 3$.

5. Weakly nonlinear theory

An examination of the numerical results of the previous section indicates that the initial fractional depth of the heavy bottom fluid plays a crucial role in determining the subsequent shape of the density interface. It appears that if $h_0 \gtrsim 0.5$ a second bore is formed behind the leading one and eventually overtakes it. However, with $h_0 \lesssim 0.5$ this second bore does not form and the gravity current remains smooth behind the front. To explore this issue and also that of linear degeneracy alluded to earlier we carry out a weakly nonlinear analysis on the model equations (3.10a,b), (3.11), and (3.12). These model equations are

$$u_t + (u + \eta_u)u_x + (1 + \eta_h)h_x = 0, \tag{3.10a}$$

$$h_t + (hu)_x = 0, \tag{3.10b}$$

$$\eta = -h^2/2 - hu^2/(1 - h), \tag{3.11}$$

$$u_1 = hu/(h - 1), \tag{3.12}$$

and for our purpose here we may discard (3.12).

With the idea of exploring the effect of initial fractional depth of the bottom fluid on the subsequent propagation of the gravity current we set

$$h(x, t) = h_0 + \tilde{h}(x, t), \qquad u = \tilde{u}(x, t) \tag{5.1}$$

in

$$\eta_u = -\frac{2hu}{1 - h}, \qquad \eta_h = -h - \frac{u^2}{(1 - h)^2}$$

and retain only the linear terms obtaining

$$\eta_u = -\frac{2h_0 u}{1 - h_0}, \qquad \eta_h = -h_0 - h, \tag{5.2}$$

where tildes have been dropped. Inserting (5.2) into (3.10a,b) our model equations have now become the quadratically nonlinear system

$$u_t + \frac{1 - 3h_0}{1 - h_0} uu_x + (1 - h_0 - h)h_x = 0, \tag{5.3a}$$

$$h_t + (h_0 + h)u_x + uh_x = 0. \tag{5.3b}$$

Our weakly nonlinear approach that we employ here provides the first nonlinear correction to the linear solution of the model equations. This correction although initially small has a profound cumulative effect in that, unlike for the linear problem, smooth initial data will result in the formation of shocks (bores).

Linearizing the model equations (5.3a,b) gives

$$u_t + (1 - h_0)h_x = 0, \tag{5.4a}$$

$$h_t + h_0 u_x = 0. \tag{5.4b}$$

Assuming a wave-like solution of the form

$$h(x, t) = h(\xi), \qquad u(x, t) = u(\xi), \qquad \xi = x - ct, \tag{5.5}$$

we have

$$\begin{bmatrix} -c & 1 - h_0 \\ h_0 & -c \end{bmatrix} \begin{bmatrix} u_\xi \\ h_\xi \end{bmatrix} = \mathbf{0}, \tag{5.6}$$

which for nontrivial solutions gives that

$$c = \pm[h_0(1 - h_0)]^{1/2}. \tag{5.7}$$

Combining the model equations of (5.3a,b) into a single equation then gives the second-order equation

$$h_{tt} - h_0(1 - h_0)h_{xx} = -(hu)_{xt} - h_0(hh_x)_x + h_0 \frac{(1 - 3h_0)}{1 - h_0}(uu_x)_x. \tag{5.8}$$

We now introduce the linear phase variables ξ and η together with a slow time variable T and make explicit the nature of the perturbation being considered. Thus we take

$$\begin{aligned} &\xi = x - ct, && \eta = x + ct, \\ &T = \varepsilon t, \\ &h = \varepsilon \tilde{h}(\xi, \eta; T), && u = \varepsilon \tilde{u}(\xi, \eta; T), \end{aligned} \tag{5.9}$$

where $c = [h_0(1 - h_0)]^{1/2}$ is the linear phase speed. Our variables transform according to

$$\begin{aligned} &\partial_t \mapsto c(\partial_\eta - \partial_\xi) + \varepsilon \partial_T \\ &\partial_x \mapsto \partial_\eta + \partial_\xi, \end{aligned} \tag{5.10}$$

and (5.8) transforms to

$$\begin{aligned} &-4c^2 h_{\xi\eta} + 2\varepsilon c(\partial_\eta - \partial_\xi)h_T \\ &\quad = -\varepsilon c(\partial_{\eta\eta} - \partial_{\xi\xi})(hu) - \varepsilon h_0(\partial_\eta + \partial_\xi)[h(h_\eta + h_\xi)] \\ &\qquad + \varepsilon h_0 \frac{(1 - 3h_0)}{1 - h_0}(\partial_\eta + \partial_\xi)[u(u_\eta + u_\xi)] + O(\varepsilon^2), \end{aligned} \tag{5.11}$$

where tildes have been dropped.

From the model equations we see that

$$c(\partial_\eta - \partial_\xi)u = -(1-h_0)(\partial_\eta + \partial_\xi)h + O(\varepsilon), \tag{5.12}$$

which leads us to consider the expansions

$$h = h^{(0)}(\xi, \eta; T) + \varepsilon h^{(1)}(\xi, \eta; T) + O(\varepsilon^2), \tag{5.13a}$$

$$u = u^{(0)}(\xi, \eta; T) + \varepsilon u^{(1)}(\xi, \eta; T) + O(\varepsilon^2). \tag{5.13b}$$

Substitution of these expansions into (5.11) and (5.12) leads to a hierarchy of problems the first two of which are:

$O(1)$ problem:

$$h^{(0)}_{\xi\eta} = 0 \tag{5.14}$$

$$c(\partial_\eta - \partial_\xi)u^{(0)} = -(1-h_0)(\partial_\eta + \partial_\xi)h^{(0)}. \tag{5.15}$$

$O(\varepsilon)$ problem:

$$\begin{aligned} -4c^2 h^{(1)}_{\xi\eta} = &-2c(\partial_\eta - \partial_\xi)h^{(0)}_T - c(\partial_{\eta\eta} - \partial_{\xi\xi})(h^{(0)}\mu^{(0)}) \\ &-h_0(\partial_\eta + \partial_\xi)[h^{(0)}(h^{(0)}_\eta + h^{(0)}_\xi)] \\ &+\frac{h_0(1-3h_0)}{1-h_0}(\partial_\eta + \partial_\xi)[u^{(0)}(u^{(0)}_\eta + u^{(0)}_\xi)]. \end{aligned} \tag{5.16}$$

The $O(1)$ problem can be solved immediately to give

$$h^{(0)} = \varphi(\xi, T) + \psi(\eta, T) \tag{5.17}$$

together with

$$u^{(0)} = \frac{1-h_0}{c}\,\varphi(\xi, T) - \frac{1-h_0}{c}\,\psi(\eta, T). \tag{5.18}$$

Employing these results in the $O(\varepsilon)$ problem gives for (5.16)

$$-4c^2 h^{(1)}_{\xi\eta} = A(\xi, T) + B(\xi, \eta, T) + C(\eta, T), \tag{5.19}$$

where

$$A(\xi, T) \equiv 2c\varphi_{T\xi} + \frac{3(1-2h_0)}{2}(\varphi^2)_{\xi\xi}, \tag{5.20}$$

$$B(\xi, \eta, T) \equiv -(1-2h_0)[\varphi\psi_{\eta\eta} + \varphi_{\xi\xi}\psi + 2\varphi_\xi\psi_\eta], \tag{5.21}$$

$$C(\eta, T) \equiv -2c\psi_{T\eta} + \frac{3(1-2h_0)}{2}(\psi^2)_{\eta\eta}. \tag{5.22}$$

The solvability conditions then require that $A \equiv 0$, $C \equiv 0$ but *not* $B \equiv 0$.

From the solvability conditions we then have equations for φ and ψ, that is,

$$\varphi_T + \frac{3(1-2h_0)}{2[h_0(1-h_0)]^{1/2}}\varphi\varphi_\xi = 0, \tag{5.23}$$

and

$$\psi_T - \frac{3(1-2h_0)}{2[h_0(1-h_0)]^{1/2}}\psi\psi_\eta = 0. \tag{5.24}$$

In deriving (5.23) and (5.24) we employed the assumption that both φ and ψ are compactly supported with respect to their spatial coordinates.

It is possible to solve the initial value problems for the equations (5.23) and (5.24) by means of the method of characteristics. These equations are forms of the inviscid Burger's equation treated, for example, in [24].

The initial value problem for φ consists of (5.23) together with the initial condition

$$\varphi(\xi, 0) = f(\xi). \tag{5.25}$$

The exact (implicit) solution can be written as

$$\varphi(\xi, T) = f(\tau) \tag{5.26}$$

on the curve

$$\xi = \frac{3(1-2h_0)T}{2[h_0(1-h_0)]^{1/2}} f(\tau) + \tau, \tag{5.27}$$

where τ is a parameter identifying each member of the family of characteristics. The condition for a shock to form is $|\varphi_\xi| \to \infty$, where

$$\varphi_\xi = \frac{2f'(\tau)[h_0(1-h_0)]^{1/2}}{3(1-2h_0)Tf'(\tau) + 2[h_0(1-h_0)]^{1/2}}, \tag{5.28}$$

and this derivative becomes infinite when

$$T = \frac{-2[h_0(1-h_0)]^{1/2}}{3(1-2h_0)f'(\tau)}. \tag{5.29}$$

The time of first breaking is therefore given by

$$T_s \equiv \min_\tau \left\{ \frac{-2[h_0(1-h_0)]^{1/2}}{3(1-2h_0)f'(\tau)} \right\}. \tag{5.30}$$

It can be seen that when $h_0 < \frac{1}{2}$ the shock will occur where $f'(\tau) < 0$, that is, on the front side, whereas if $h_0 > \frac{1}{2}$ then shock occurs where $f'(\tau) > 0$.

The initial value problem for ψ consists of (5.24) together with the initial condition

$$\psi(\eta, 0) = g(\eta). \tag{5.31}$$

The exact solution can be written as

$$\psi(\eta, T) = g(\tau) \tag{5.32}$$

on

$$\eta = \frac{-3(1-2h_0)T}{2[h_0(1-h_0)]^{1/2}}\, g(\tau) + \tau \tag{5.33}$$

and the time of first shock formation calculated as

$$T_s \equiv \min_{\tau} \left\{ \frac{2[h_0(1-h_0)]^{1/2}}{3(1-2h_0)g'(\tau)} \right\}. \tag{5.34}$$

Thus if $h_0 < \frac{1}{2}$ the shock occurs where $g'(\tau) > 0$ and if $h_0 > \frac{1}{2}$ the shock occurs where $g'(\tau) < 0$.

The analysis of this section tends to confirm what we observed in the numerical experiments of the previous section. That is, a smooth wave propagating to the right has the possibility of forming a bore at its trailing edge only if the unperturbed fractional depth of the heavy fluid exceeds the value $\frac{1}{2}$. The experiments of Rottman and Simpson [13] tend also to confirm the existence of such a critical value for h_0 although it is very difficult to get an accurate estimation of it from the experiments.

It may also be seen from either (5.30) or (5.34) that when $h_0 \to \frac{1}{2}$ the time of shock formation becomes infinite. This is the effect of the linear degeneracy in the vicinity of $u = 0$, $h = \frac{1}{2}$.

6. Concluding remarks

In this paper we have presented both numerical and analytical analyses for an important class of problems involving the unsteady motion of one fluid within another when this motion is driven by density differences alone. Our weak stratification model developed here is tested against the model equations for a shallow-water two-fluid system and shown to capture the essential dynamics of the flow as well as being amenable to an analytical treatment. This analytical treatment has enabled us to determine that there is a critical value for the initial fractional depth occupied by the heavy fluid below which shocks (bores) do not form on the trailing edge.

References

1. J. E. SIMPSON, Gravity currents in the laboratory, atmosphere, and ocean, *Ann. Rev. Fluid Mech.* **14**: 213–234 (1982).
2. W. A. LYONS and C. S. KEEN, Computed 24-hour trajectories for aerosols and gases in a lake/land breeze circulation cell on the western shore of Lake Michigan, *6th Conference on Weather Forecasting, Albany, NY*, pp. 78–83, 1976.
3. G. W. SCHAEFER, An airborne radar technique for the investigation and control of migrating pest insects, *Philos. Trans. Roy. Soc. London Ser. B* **287**: 459–465 (1979).
4. P. D. KOMAR, Comparisons of the hydraulics of water flows in Martian outflow channels with flows of similar scale on Earth, *Icarus* **37**: 156–181 (1979).
5. T. VON KÁRMÁN, The engineer grapples with nonlinear problems. *Bull. Am. Math. Soc.* **46**: 615–683 (1940).
6. T. B. BENJAMIN, Gravity currents and related phenomena, *J. Fluid Mech.* **31**: 209–248 (1968).
7. G. H. KEULEGAN, The motion of saline fronts in still water, *Nat. Bur. Stand. Rest.* 5831 (1958).
8. B. J. DALY and W. E. PRACHT, Numerical study of density-current surges, *Phys. Fluids* **11**: 15–30 (1968).
9. G. V. MIDDLETON, Experiments on density and turbidity currents II. Uniform flow of density currents, *Canad. J. Earth Sci.* **3**: 627–637 (1966).
10. T. W. KAO, C. PARK, and H-P. PAO, Inflows, density currents, and fronts, *Phys. Fluids* **21**: 1912–1922 (1978).
11. H. E. HUPPERT and J. E. SIMPSON, The slumping of gravity currents, *J. Fluid Mech.* **99**: 785–799 (1980).
12. G. H. KEULEGAN, An experimental study of the motion of saline water from locks into fresh water channels, *Nat. Bur. Stand. Rep.* 5168 (1957).
13. J. W. ROTTMAN and J. E. SIMPSON, Gravity currents produced by instantaneous releases of a heavy fluid in a rectangular channel, *J. Fluid Mech.* **135**: 95–110 (1983).
14. R. E. GRUNDY and J. W. ROTTMAN, The approach to self-similarity of the solutions of the shallow-water equations representing gravity-current releases, *J. Fluid Mech.* **156**: 39–53 (1985).
15. J. PEDLOSKY, *Geophysical Fluid Dynamics*, Springer-Verlag, Berlin/New York, 1987.
16. P. D. LAX, *Hyperbolic Systems of Conservation Laws and the Mathematical Theory of Shock Waves*, SIAM, 1973.
17. Y. HE and T. B. MOODIE, Scalar conservation laws and spatially dependent flux functions, *Stud. Appl. Math.* **91**: 215–245 (1994).
18. Y. HE and T. B. MOODIE, 1991. The signaling problem in nonlinear hyperbolic wave theory, *Stud. Appl. Math.* **85**: 343–372 (1991).
19. R. LEVEQUE, *Numerical Methods for Conservation Laws*, Birkhäuser, 1992.
20. A. LAPIDUS, A detached shock calculation by second-order finite differences, *J. Comp. Phys.* **2**: 154–177 (1967).
21. T. K. FANNELOP and G. D. WALDMAN, Dynamics of oil slicks, *AIAA J.* **10**: 506–510 (1972).
22. D. P. HOULT, Oil spreading on the sea, *Ann. Rev. Fluid Mech.* **4**: 341–368 (1972).

23. P. GLAISTER, Flux splitting for hyperbolic systems of conservation laws with source terms, *Comput. Math. Appl.* **26**, No. 7: 79–96 (1993).

24. G. B. WHITHAM, Linear and Nonlinear Waves, Wiley-Interscience, 1974.

UNIVERSITY OF ALBERTA, EDMONTON

(Received January 20, 1995)